The effect of processing conditions on the dielectric properties of doped calcium lanthanum nickelate

Yulia A. Deeva [a]* , Abdullo A. Mirzorakhimov [a] , Alexey Yu. Suntsov [b] , Nadezhda I. Kadyrova [b] , Nina V. Melnikova [a] , Tatyana I. Chupakhina [b]

a: Institute of New materials and technologies, Ural Federal University, Ekaterinburg 620009, Russia
b: Institute of Solid State Chemistry UB RAS, Ekaterinburg 620990, Russia
* Corresponding author: juliahik@mail.ru

This paper belongs to a Regular Issue.

Abstract

The influence of thermal and thermobaric (TBT) effects on the structure, microstructure, and dielectric properties of ceramics based on solid solutions of the $La_{1.8}Ca_{0.2}Ni_{0.8}M_{0.2}O_{4+\delta}$ (M = Co, Cu) composition was studied. TBT treatment of the samples leads to a change in the grain morphology of ceramics and an increase in the dielectric constant compared to its value only after heat treatment. The change in the anisotropy of the coordination $(La,Ca)O_9$ and $(Ni,M)O_6$ polyhedra after TBT contributed to interlayer polarization in the crystal structure of $La_{1.8}Ca_{0.2}Ni_{0.8}M_{0.2}O_{4+\delta}$.

1. Introduction

The search for materials with a high dielectric constant and low dielectric losses is one of the main tasks of modern materials science. However, this problem does not have a simple solution since an increase in the dielectric constant (ε) is accompanied by an increase in dielectric losses (tan δ) and the dependence of dielectric parameters on temperature.

For the first time, a very high value of the permittivity was found in single crystals of layered perovskite-like oxides, such as $CaCu_3Ti_4O_{12}$, $La_{15/8}Sr_{1/8}NiO_4$ (structural type K_2NiF_4, for oxides – A_2BO_4) and solid solutions based on them; the value was ε is very large [1, 2]. In the lanthanum-strontium nickelate, this characteristic is frequency- and temperature independent, which makes this material promising for practical applications ($\varepsilon \sim 10^5–10^6$) [3, 4]. In ceramic samples and thin films of $CaCu_3Ti_4O_{12}$ and $La_{15/8}Sr_{1/8}NiO_4$, the dielectric constant has a lower value and decreases with an increase in the frequency of the electric field [3, 5]. It was found that the ceramics obtained by the thermobaric method have better dielectric characteristics in comparison with those of the samples obtained by the ceramic technology at atmospheric pressure [6, 7]. At a low frequency (10^2 Hz), the dielectric constant and dielectric losses of $CaCu_3Ti_4O_{12}$ (CCTO) increase with an increase in the calcination temperature and an increase in the grain size [8]. Thus, CCTO had the highest dielectric constant and tan δ values. At the middle frequency ($10^3–10^5$ Hz), CCTO was found to exhibit the lowest tan δ value (0.091).

Among ceramics based on complex oxides with a structure of the type K_2NiF_4 (for oxides, the formula is written as A_2BO_4), which have been extensively researched over the past decade, the compounds with both temperature- and frequency-independent giant dielectric constant ($Ln_{2-x}Sr_xNi_{1-y}M_yO_4$ (Ln – rare earth element (REE), M = Co, Cu; $\varepsilon \sim 10^3–10^6$, tan δ>1.0), and with a low tangent of the dielectric loss angle ($A_{2-x}Ln_xTi_{1-y}M_yO_4$ (A = Ca, Sr); $\varepsilon \sim 10$–30, tan δ<10^{-3}) were found [9].

It is known that a high dielectric constant in REE-strontium layered nickelates is realized due to interlayer charge polarization, which is influenced by structural anisotropy. Structural distortions of the AO_9 and BO_6 coordination polyhedra can be regulated by partial or complete substitution of cations in the position A. The dielectric response suddenly changes with changing the rare earth ion, when the crystal symmetry changes, so there should be a link between the dielectric response and crystal symmetry [6, 10]. Of the unsubstituted nickelates, the $Sm_{1.5}Sr_{0.5}NiO_4$ compound has the best characteristics ($\varepsilon = 10^6$, tan δ<0.1), but these parameters are unstable and depend on the temperature and frequency of the electric field [11]. It should be noted that the difference between the radii of Sm and Sr (coordination number of which is IX) leads to the formation of an oxide with orthorhombic symmetry [12], in contrast with the analogous compounds, La-, Pr-, Nd-containing

ones, crystallizing in the tetragonal modification [13–15]. In solid solutions $(Sm_{1-x}Nd_x)_{1.5}Sr_{0.5}NiO_4$ the orthorhombic phase exists for $x<0.6$, while for $0.6<x<1.4$ the structure becomes tetragonal [16], and after this transition ε falls and tan δ increases.

The relationship between dielectric characteristics and structural anisotropy due to the replacement of La ($r = 1.31$ Å) by Ca cation ($r = 1.01$ Å) was described in [17] using the $La_{2-x}Ca_xNiO_4$ solid solution as an example. It was shown that the distortions of the AO_9 and BO_6 polyhedra change at different x, which allowed the authors to obtain a compound with a high ε ~ 10^4 ($x = 0.2$), but a rather high value of tan δ ~ 100 ($x = 0.3$). In the resulting oxides, the dielectric constant strongly depends on frequency and temperature, which is unusual for compounds of this class. There are no other data on the dielectric properties of Ca-substituted nickelates of lanthanum and other rare-earth elements in the literature.

On the other hand, the parameters of the A_2BO_4 structure change upon partial substitution of elements located not only in the A position, but also in the B position, especially if the substitution is heterovalent. In this case, the interlayer polarization is affected not only by structural distortions, but also by the charge state of the cations that make up the oxide [18].

Investigation of the dielectric characteristics of $(La,Ca)(Ni,M)O_4$ (M = Cu, Co) ceramics, the results of which we present in this work, was aimed at studying the nature of high dielectric permittivity in layered perovskite-type oxides with a K_2NiF_4 type structure.

The choice of Co and Cu as substitute elements is due to the Jahn-Teller nature of the Cu^{2+} cation and the preferred oxidation state of Co^{3+} at high temperatures, which should have a significant effect on the structural anisotropy. Elongations of BO_6 octahedra along the c axis in the presence of Cu^{2+} in position B, as shown in [19], stabilizes the frequency-independent behavior of the dielectric constant in lanthanum-strontium nickelates, and the presence of Co^{3+} increases the dielectric constant [6].

Another, no less important task of this study was to investigate the influence of the sample morphology on the dielectric characteristics.

Thermobaric treatment changes the microstructure of the samples, which has a noticeable effect on the dielectric properties of ceramics based on oxide compounds. Strong influence on the dielectric parameters is exerted by the Maxwell-Wagner polarization at grain boundaries and inhomogeneities. This effect refers to external factors that affect the dielectrics parameters value.

In this paper, ceramic samples of K_2NiF_4 structural type, which have a composition $La_{1.8}Ca_{0.2}Ni_{0.8}M_{0.2}O_{4+\delta}$ (M = Co, Cu) were investigated. To improve the dielectric properties of ceramics based on the complex oxides, the anisotropy of coordination polyhedra was controlled by conjugated substitution of the cationic positions of Ln and 3d-metals, the shape and particle size distribution of crystallites were formed using the precursor method for the synthesis of ultrafine powders and subsequent thermobaric treatment.

2. Experimental

For the formation of single-phase solid solutions of the composition $La_{1.8}Ca_{0.2}Ni_{0.8}M_{0.2}O_{4+\delta}$ (M = Co, Cu), we employed the precursor synthesis method described in detail in [6] using 2-substituted ammonium citrate ($C_6H_{14}N_2O_7$).

$La(NO_3)_3 \cdot 6H_2O$, $CaCO_3$, NiO, CoO and CuO of the "extra pure" qualification were used as starting reagents. The oxides and carbonates were dissolved in concentrated nitric acid, and the nitrates – in distilled water. The solutions were mixed, and a 1.5-fold excess of the organic component was added. The resulting homogeneous solution was evaporated at 673 K until the reaction mixture ignited.

Thermal treatment of the obtained pyrolysis product was carried out in two stages: at 873 K for 5 h to remove the residual organic products and at 1323 K for 16 h to complete the phase formation process. The phase analysis of the reaction products was performed using the crystallographic database "Database of Powder Standard – PDF2" (ICDD, USA, Release 2009 [card 00-024-1326]).

To form ceramic samples, the obtained single-phase finely dispersed black powder was pressed at a pressure of 9.5 MPa into tablets 10 mm in diameter and sintered at 1523 K for 8 h.

The composition of the obtained samples was controlled using a Shimadzu XRD-7000 S automatic diffractometer with 0.03° step in the 10–120° range with 3–5 s exposure per point. X-ray pattern processing was performed with a FULLPROF-2019 program. The shape and average size of particles of the samples under investigation were determined by scanning electron microscopy on a JEOL JSM 6390 scanning electron microscope with an attachment for energy dispersive analysis of JED 2300 in the BES mode at a x3000 magnification.

The determination of the thermal expansion coefficient of the samples under study was carried out on a Netsch DIL 402 C dilatometer in an argon atmosphere. The maximum temperature was 1720 K.

The measurements of oxygen content in the obtained specimens were carried out by thermogravimetry (TG) technique with the use of a TG-92 Setaram analyzer. For the thermal analysis, about 0.2 g of the pulverized material was placed in the corundum pan, heated, and kept in air at 1223 K for 2 h. Then the sample was slowly cooled down to 423 K with the rate of 1°/min. Such preliminary procedure is believed to provide a total removal of surface adsorbates and to achieve equilibrium values of oxygen content in oxides in the cooling mode. Then the atmosphere was switched to Ar diluted by 5 vol.% H_2 and the samples were heated up to 1223 K until an exhaustive oxygen loss was achieved. Such procedure resulted in the reduction of the sample to the powder mixture of La_2O_3, CaO, Co and Cu. The respective weight loss was used for calculations of the total oxygen content ($4\pm\delta$) in the as-synthesized samples.

Thermobaric treatment of ceramic samples was carried out in a "toroid" high-pressure chamber on a DO-137A press at a pressure of 2.5 and 4 GPa for 5 minutes at 1173 K. To prevent carbon contamination of the sample, the internal walls of the heater were covered with platinum foil.

Dielectric characteristics were measured using a universal analyzer of the frequency response of an impedance meter/dielectric spectrometer Solartron 1260A functioning in the frequency range 1 mHz–30 MHz. The frequency dependence of the dielectric constant was estimated in the frequency range from 1 kHz to 1 MHz.

Temperature examinations of electrical characteristics of samples in the range 10–300 K were carried out in pure helium atmosphere in an autonomous closed cycle cryostat with the DE-204SL two-stage cryorefrigerator, based on Gifford-Macmagon cycle using a helium water-cooled compressor. The accuracy of cryogenic temperature measurements was 0.2 K.

3. Results and Discussion

3.1. Synthesis and structural characteristics of complex oxide $La_{1.8}Ca_{0.2}Ni_{0.8}M_{0.2}O_{4+\delta}$ (M = Co, Cu). Microstructural analysis of the obtained ceramic samples

For the synthesis of powdered oxides of the $La_{1.8}Ca_{0.2}Ni_{0.8}M_{0.2}O_{4+\delta}$ (M = Co, Cu) composition, the "solution combustion" method was used [20–22]. The choice of diammonium citrate as an organic component ensures the formation of citrates of the corresponding metals and the release of NH_4NO_3 into the reaction zone [19]. The interaction of ammonium nitrate with organic components of the reaction mixture provides the ignition of the solution, accompanied by decarboxylation.

Pyrolysis of a reaction mass containing nitrogen in a reduced form proceeds with the formation of nanodispersed powders with a developed surface and high reactivity [23]. The high dispersion of the studied powders contributes to better sintering of ceramics and the absence of through and closed pores.

Figure 1 illustrates the results of thermogravimetry experiments. As can be seen, the studied oxides start to lose oxygen at 550 K and 650 K for the copper- and cobalt-doped samples, respectively. Earlier, a mechanism for the reduction of the copper-containing nickelate was considered in the literature [24–26] where two steps were also observed. The first one is related to the formation of the stoichiometric phase. At higher temperatures, deeper decomposition takes place, resulting in the formation of metals and simple oxides. XRD analysis of the reduced mixtures fully supports this point of view.

It is important that the studied oxides remain stable in Air media where negligible changes in oxygen content are observed. At the same time, the cobalt-containing sample is characterized by elevated oxygen content compared with copper doped one which may indicate the formation of more oxidized forms such as Co^{3+}.

To determine the effect of particle morphology on dielectric properties, the formation of ceramics was carried out in two ways: heat treatment of the precursor in the air and thermobaric treatment (TBT) of the precursor.

### 3.1.1. Heat treatment of the precursor in the air

Figure 2 shows the dilatometric measurement data for the obtained powder samples. It can be seen from the plots that the sintering process of both samples begins at a temperature in the range from 1155 K to 1280 K.

Figure 3 shows SEM images of ceramics obtained after heat treatment at 1523 K. The countable size distribution of crystallites is presented in the form of a histogram (Figure 3 (inset)) expressing the percentage of grains with sizes lying in these intervals.

The surface of ceramic samples (Figures 3a and 3b) is densely sintered i.e. has no through pores. Crystallites of ceramic samples in both cases have a poorly crystallized shape with a not clearly pronounced growth zone. However, the sample containing Co has a more faceted lamellar shape compared to the sample containing Cu. The average crystallite size for both samples is about 3 μm. Nevertheless, it should be noted that in the ceramics with Co the particles are more dispersed than in the sample containing Cu.
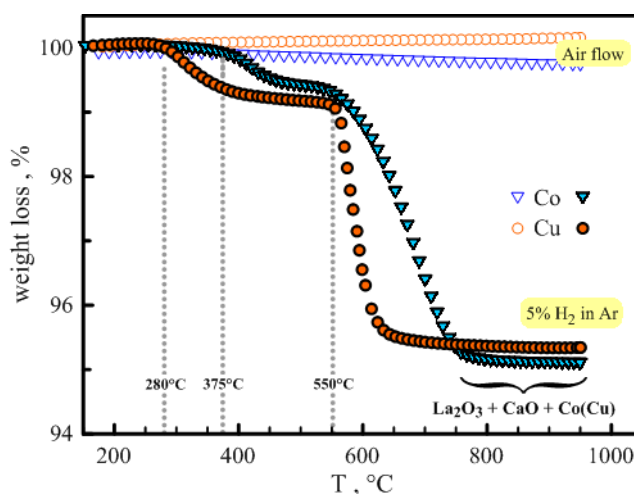
Figure 1 Variations of oxygen content in $La_{1.8}Ca_{0.2}Ni_{0.8}M_{0.2}O_{4\pm\delta}$ (M = Cu, Co) measured in Air flow and Ar diluted by 5 vol.% H_2. The represented data were collected in cooling and heating modes, respectively.
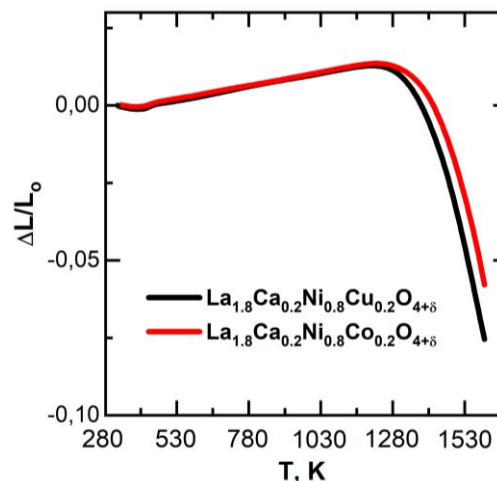
Figure 2 Kinetic curves of sintering complex oxides of $La_{1.8}Ca_{0.2}Ni_{0.8}M_{0.2}O_{4\pm\delta}$ (M = Cu, Co) composition.
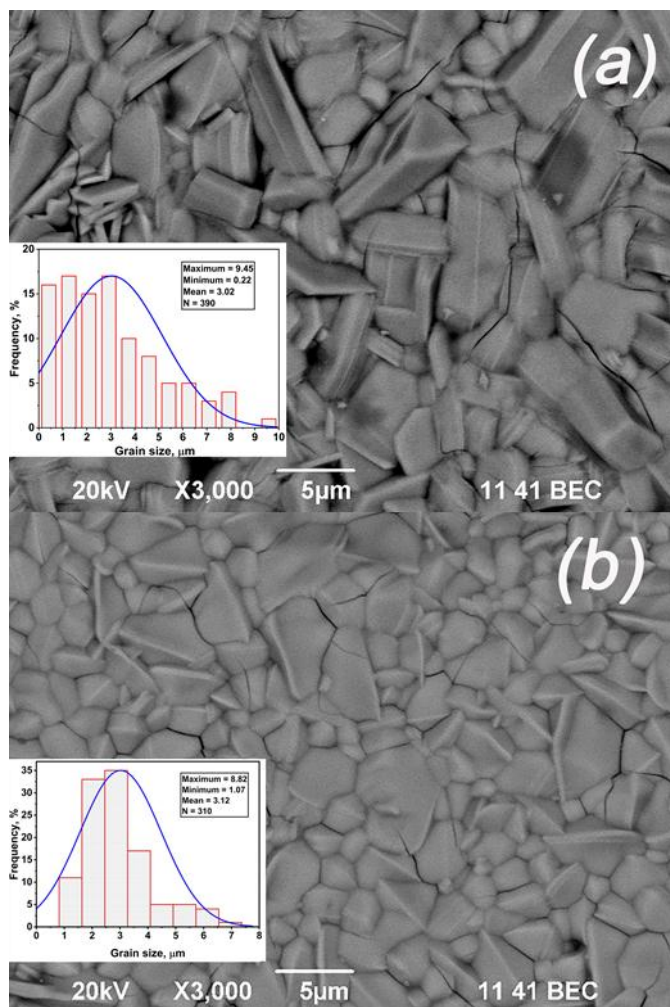
Figure 3 SEM micrographs of the $La_{1.8}Ca_{0.2}Ni_{0.8}M_{0.2}O_{4+\delta}$ (M = Co (a), Cu (b)) ceramics surface obtained after heat treatment (sintering) (the inset shows the crystallite size distribution).

Figure 4 SEM micrographs of the $La_{1.8}Ca_{0.2}Ni_{0.8}M_{0.2}O_{4+\delta}$ (M = Co (a), Cu (b)) ceramics surface obtained after TBT (the inset shows the crystallite size distribution).

3.1.2. Thermobaric treatment (TBT) of the precursor

Significant changes in the morphology of ceramics are observed after treatment of precursors simultaneously with temperature and pressure (TBT) (Figure 4). The morphology of crystallites changes significantly, acquiring a more faceted shape, and the particle size decreases for both samples by approximately a factor of 2 (Figure 4 (insets)).

The influence of the morphology of ceramics after TBT on the dielectric properties and the regularities of changes in the shape of crystallites are poorly studied. In [27] the effect of TBT on ceramics with the composition $CaCu_3Ti_4O_{12}$ leads to an increase in the particle size and to the absence of a visible change in grain morphology. In contrast, after TBT in the $La_{1.8}Ca_{0.2}Ni_{0.8}M_{0.2}O_{4+\delta}$ (M = Co, Cu) compounds the ceramic grain morphology changes rather strongly (Figure 4 (a) and (b)). It can be assumed that the shape and size of crystallites after TBT depend on the type of crystal lattice of the compound under study.

The phase composition of the obtained ceramic samples was determined based on the results of X-ray phase analysis (Figure 5).

The results of phase analysis of the obtained ceramic indicate the absence of foreign phases; this is proven by the correspondence of the X-ray diffraction reflections with the Miller indices (*hkl*) of the structure of the Ruddlesden–Popper phase.

Since, in oxides with a structure of the K_2NiF_4 type, there is a correlation between the dielectric properties and distortion of the antiprisms of AO_9 and octahedra BO_6 [17, 28, 29], the crystal chemical parameters of all the samples under study were determined. Table 1 shows the crystallochemical parameters of the test compounds before and after TBT.

To analyze the structural distortions of the compounds under study before and after TBT, Figure 6 shows a graph of normalized bond lengths, i.e., the ratio of the experimental interatomic distances to the theoretical sum of ion radii (according to Shannon [30]) in the corresponding coordination (l_{exp}/l_{theor}). The coordination polyhedra $(La,Ca)O_9$ and $(Ni,M)O_6$ are shown in the crystal structure (Figure 7).

According to the literature date [27, 31], thermobaric treatment at temperatures up to 1200 K does not lead to a change in the space group of crystalline substances. However, structural deformation can occur, which can have a significant effect on material properties, such as magnetic or electrical.
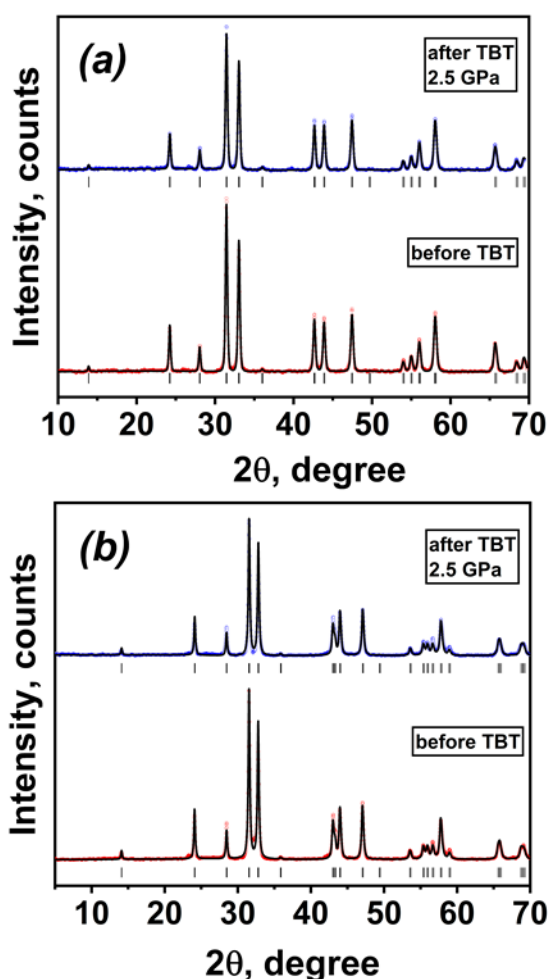
Figure 5 Theoretical and experimental diffraction patterns of the La$_{1.8}$Ca$_{0.2}$Ni$_{0.8}$M$_{0.2}$O$_{4+\delta}$ (M = Cu (a), Co (b)) ceramics obtained before and after thermobaric treatment. The Bragg reflections positions are marked with dashes.
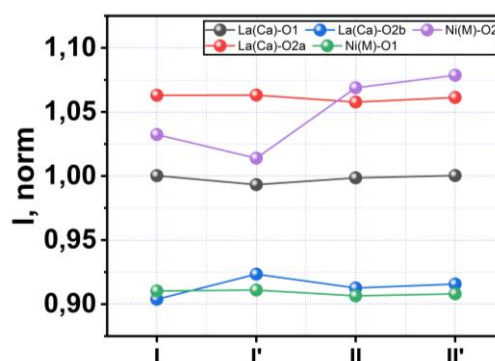

Figure 6 Normalized bond lengths values in coordination polyhedra (La,Ca)O$_9$ and (Ni,M)O$_6$ of the composition La$_{1.8}$Ca$_{0.2}$Ni$_{0.8}$M$_{0.2}$O$_{4+\delta}$ (M = Co (I), Cu (II)) compounds, where I' and II' – samples after TBT at P = 2.5 GPa.
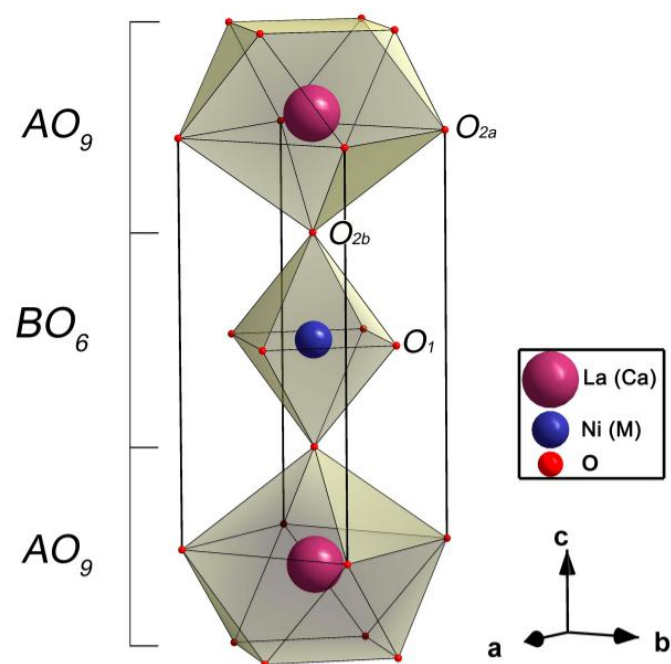
Figure 7 Crystallographic structure of La$_{1.8}$Ca$_{0.2}$Ni$_{0.8}$Co$_{0.2}$O$_{4+\delta}$. The La and Ca atoms are represented by purple, Ni and M – by dark blue, oxygen – by red spheres.

According to the data obtained (Figure 6), the strongest structural change after TBT is manifested along the *c* axis (the La (Ca)–O2b bond in the AO$_9$ coordination polyhedron and the Ni(M)–O2b bond in BO$_6$) for both samples. However, it is important to note that in the case of the sample containing Cu in position B (sample II'), the BO$_6$ octahedron becomes more distorted, while the sample containing Co, on the contrary, after TBT, approaches the ideal lattice state.

According to [32] the presence of Jahn-Teller ions in the composition of perovskite-type oxides provides the greatest response of structural distortions to thermobaric action.

3.2. Temperature dependences of the electrical properties of materials at different frequencies

The impedance hodographs (Figure 8) are the arcs of semicircles whose ReZ intercepts correspond to the resistance of grain boundaries.

The impedance hodographs for samples in all temperature range are arcs of semicircles, the radii of which monotonously decrease with increasing temperature, which indicates a decrease in electrical resistance of the grain boundaries.

The presence of one arc on the impedance hodographs of the studied materials indicates that the processes occurring in an alternating field can be characterized by a single relaxation time or that the relaxation times of carriers and polarization relaxation processes are distributed in a certain narrow interval.

The frequency dependences of the imaginary part of the electric modulus for the studied samples at some temperatures are shown in Figure 9 (for La$_{1.8}$Ca$_{0.2}$Ni$_{0.8}$Cu$_{0.2}$O$_{4+\delta}$ samples) and Figure 10 (for La$_{1.8}$Ca$_{0.2}$Ni$_{0.8}$Co$_{0.2}$O$_{4+\delta}$ samples). The polarization relaxation time (τ) was determined using the frequency values f_{max} corresponding to the maximum point of the graph ImM(f) plot using the equation:

$$\tau = 1/2\pi f_{max}. \qquad (1)$$

Table 1 Crystallo chemical parameters of $La_{1.8}Ca_{0.2}Ni_{0.8}M_{0.2}O_{4+\delta}$ (M = Co (I), Cu (II)) samples (space group $I4/mmm$, La/Ca (0, 0, z), Ni/M (0, 0, 0), O(1) (0, 0.5, 0); O(2) (0, 0, z)).

Samples	I	I' (2.5 GPa)	II	II' (2.5 GPa)
Unit cell parameters				
$a = b$, Å	3.8552(2)	3.8580(2)	3.8257(4)	3.8328(1)
c, Å	12.5546(3)	12.5208(7)	12.7156(1)	12.7212(3)
V, Å³	186.591(4)	186.363(8)	186.110(7)	186.881(2)
Atom coordinates				
La (Ca)				
z	0.3611(8)	0.3631(5)	0.3621(4)	0.3619(2)
O1				
Occupancy	0.929(3)	0.902(8)	0.993(8)	0.889(6)
O2				
z	0.1740(7)	0.1715(9)	0.1757(8)	0.1788(1)
Occupancy	0.946(4)	1.086(7)	1.018(6)	1.090(3)
$\chi2$	0.781	0.937	0.785	0.892
Interatomic distances, Å				
Ni/M–O1(x4)	1.9276(8)	1.9290(6)	1.9128(6)	1.9164(2)
Ni/M–O2b(x2)	2.186(7)	2.147(3)	2.234(4)	2.276(1)
La/Ca–O1(x4)	2.5988(7)	2.5806(12)	2.5946(12)	2.5990(17)
La/Ca –O2a(x4)	2.7617(3)	2.7622(6)	2.7481(2)	2.7573(3)
La/Ca –O2b(x1)	2.348(6)	2.399(3)	2.371(4)	2.379(7)
Rf-factor	3.98	4.32	3.40	2.65
GII	0.3909	0.8723	0.5561	0.6720
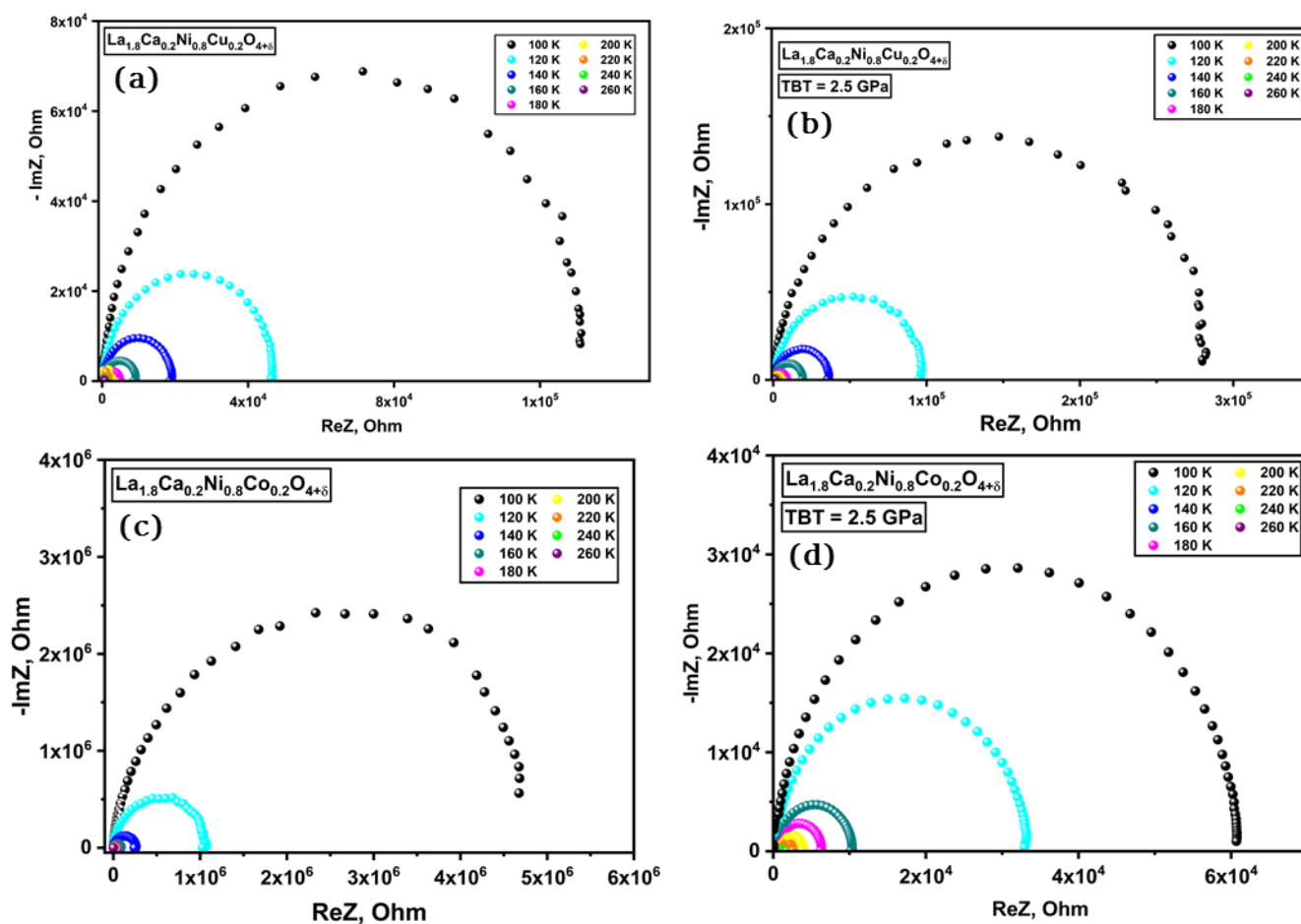
Figure 8 Impedance spectra of cells with samples $La_{1.8}Ca_{0.2}Ni_{0.8}M_{0.2}O_{4+\delta}$ (M = Co, Cu) (a, c) compounds before and after TBT at P = 2.5 GPa (b, d).
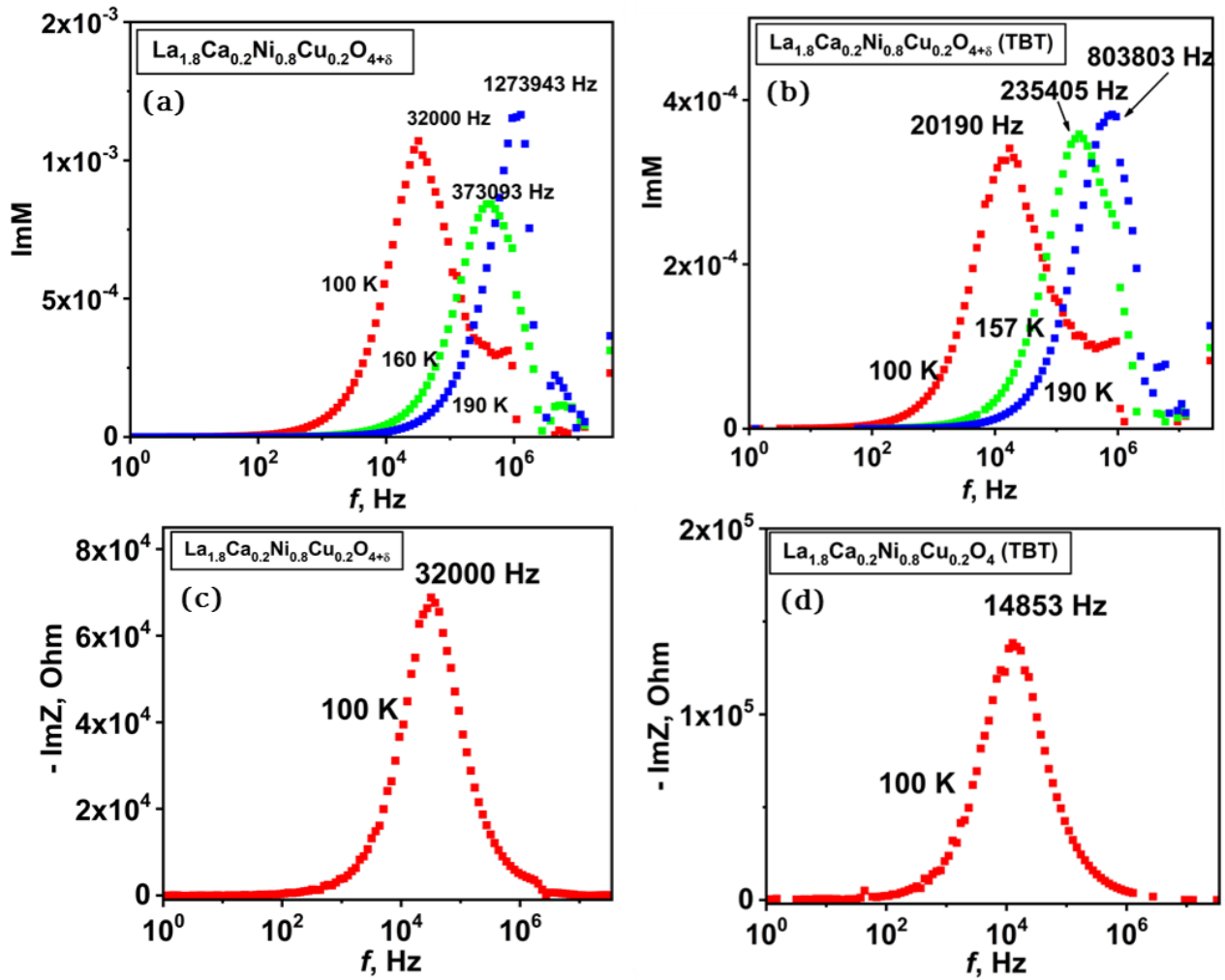
Figure 9 The frequency dependences of the imaginary part of the electric modulus for the $La_{1.8}Ca_{0.2}Ni_{0.8}Cu_{0.2}O_{4+\delta}$ samples (before (a, c) and after TBT (b, d)) at some temperatures and frequency dependences of the imaginary part of the impedance at $T = 100$ K.

The relaxation times of charge carriers from $-ImZ(f)$ at $T = 100$ K (Figure 9) are $\tau = 5.0 \cdot 10^{-6}$ s and $\tau = 1.1 \cdot 10^{-5}$ s (for before and after TBT, respectively).

For the material with copper, the relaxation times $\tau = 1/2\pi f_{max}$ after TBT slightly increase, but for the material with Co, the values τ decrease by an order of magnitude and even by two at $T \leq 100$ K.

An increase in the relaxation time after TBT can be associated with an increase in polarization in the regions of grain boundaries, the surface of which increases with a decrease in the particle size during such treatment. That is, the external causes described in the IBLC model and associated with the Maxwell-Wagner polarization mechanism play a large role in increasing the dielectric constant.

3.3. Dielectric properties of $La_{1.8}Ca_{0.2}Ni_{0.8}M_{0.2}O_{4+\delta}$ (M = Co, Cu) ceramics

The relative complex permittivity, admittance and loss tangent were estimated by measuring the impedance $Z = \text{Re } Z + i \, \text{Im} Z$ with the equation:

$$\varepsilon^*(\omega) = \frac{l}{S} \frac{1}{i\omega\varepsilon_0 Z^*(\omega)}, \tag{2}$$

$$Y^*(\omega) = \frac{1}{Z^*(\omega)}, \tag{3}$$

$$\tan \delta(\omega) = \frac{\text{Im } \varepsilon}{\text{Re } \varepsilon}, \tag{4}$$

where ω is the circular frequency ($\omega = 2\pi f$, and f is the linear frequency of electric field), ε_0 is the dielectric constant of vacuum, and l and S are the sample thickness and the surface area contacting with one electrode, respectively.

3.3.1. Dielectric characteristics of the test samples obtained after heat treatment in air

The plots of the dependence of the dielectric constant and the dielectric loss angle tangent of the $La_{1.8}Ca_{0.2}Ni_{0.8}M_{0.2}O_{4+\delta}$ (M = Co, Cu) ceramics on the frequency at different temperatures are shown in Figure 11.

The dielectric constant for both samples have high values of the order of 10^3 (M = Co) and $8 \cdot 10^2$ (M = Cu) and is frequency independent in the temperature range from 100 to 260 K. However, low values of the dielectric loss tangent are observed only in the temperature range of 100–120 K.
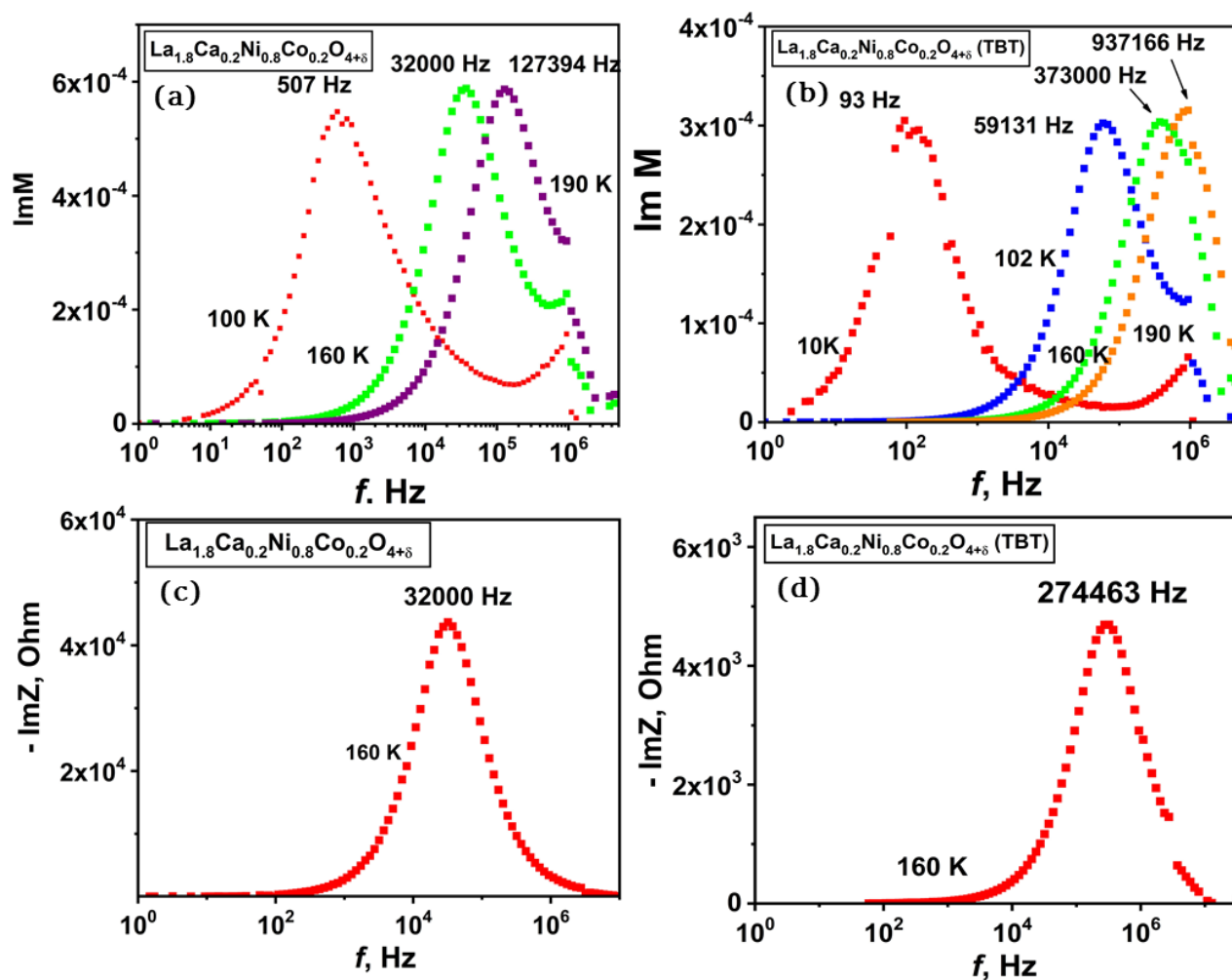
Figure 10 The frequency dependences of the imaginary part of the electric modulus for the $La_{1.8}Ca_{0.2}Ni_{0.8}Co_{0.2}O_{4+\delta}$ samples (before (a, c) and after TBT (b, d)) at some temperatures and frequency dependences of the imaginary part of the impedance at $T = 160$ K.

The appearance of sufficiently high values of the dielectric constant can be due to both external factors (near-electrode polarization effects, Maxwell-Wagner effects on grain boundaries, the influence of shape and size of grains) and internal reasons (properties of the material itself – features of the crystalline layered structure, type of charge carriers and related polarization processes).

3.3.2. Dielectric characteristics of the ceramics obtained after thermobaric treatment

The resulting dielectric data for the ceramics after TBT are shown in Figure 12. Both samples are characterized by an increase in Re ε and retention of frequency and temperature independence (in comparison with the ε value after the ceramics heat treatment). For the sample containing Cu in position B, the value of the dielectric constant increases by 200, and for M = Co – increases by 100.

The dielectric constant of the $La_{1.8}Ca_{0.2}Ni_{0.8}Cu_{0.2}O_{4+\delta}$ ceramic increases significantly after thermobaric treatment from 600 to 2000. For the $La_{1.8}Ca_{0.2}Ni_{0.8}Co_{0.2}O_{4+\delta}$ sample, the change in the dielectric constant increases from 1000 to 2000). The difference is due to a stronger distortion of the BO_6 tetrahedron in the copper-containing sample, which due to the influence of the Jahn-Teller effect.

Also , an increase increasing in the dielectric constant of $La_{1.8}Ca_{0.2}Ni_{0.8}M_{0.2}O_{4+\delta}$ (M = Co, Cu) ceramic after TBT can be associated with a change in the morphology of crystallites that acquire regular geometric flat surfaces after TBT (Figure 4), with a decrease in the average grain size (from ~3 μm to ~1.7 μm). As a consequence, this leads to more pronounced polarization effect in the region of grain boundaries with an increased total area of grain boundaries (IBLC model) [33, 34], and with an increase in the number of barriers for charge carriers in the form of surfaces of inhomogeneities, the number of which increases in the course of TBT. Thus, the increase in the values of the dielectric constant observed in the materials after TBT is mainly associated with the Maxwell-Wagner mechanism of polarization at grain boundaries and inhomogeneities.

4. Conclusions

New complex oxides of the K_2NiF_4 type with the $La_{1.8}Ca_{0.2}Ni_{0.8}M_{0.2}O_{4+\delta}$ (M = Co, Cu) composition were synthesized by pyrolysis of nitrate-organic compositions with 2-substituted ammonium citrate as an organic component, proceeding in the "solution combustion" mode.
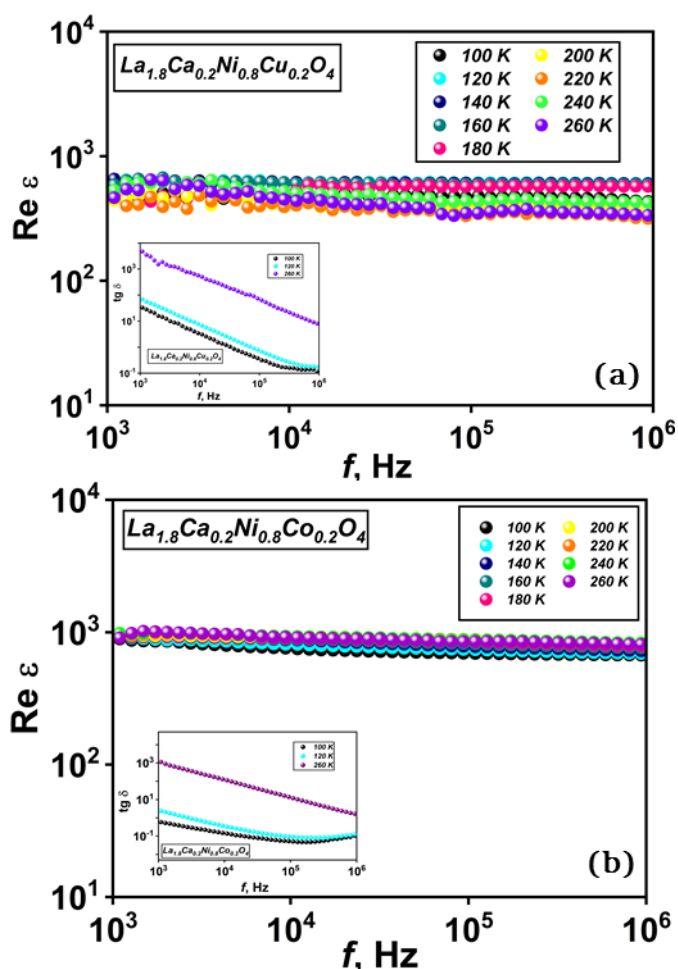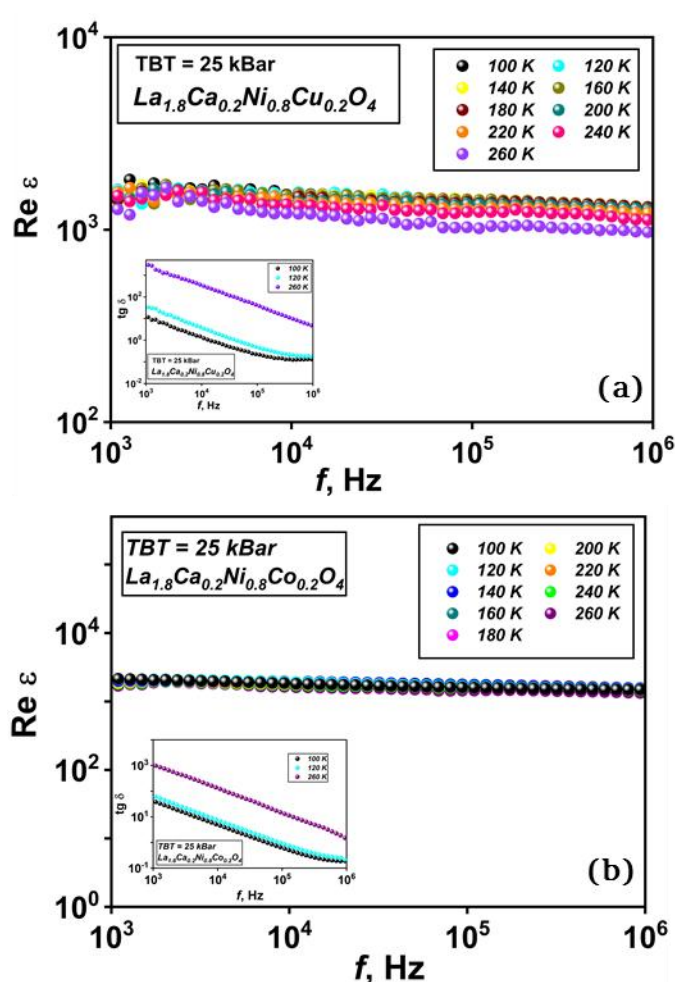
Figure 11 The frequency dependence of dielectric constant and dielectric loss tangent on temperature for $La_{1.8}Ca_{0.2}Ni_{0.8}M_{0.2}O_{4+\delta}$ (M = Cu (a), Co (b)) ceramics obtained after heat treatment in air.

Figure 12 The frequency dependence of dielectric constant and dielectric loss tangent on temperature for $La_{1.8}Ca_{0.2}Ni_{0.8}M_{0.2}O_{4+\delta}$ (M = Cu (a), Co (b)) ceramics obtained after TBT.

The transformation of the resulting precursors into the final product takes place at lower temperatures (1223 K) compared to the solid-phase method (1473 K), which solves the problem of obtaining nanodispersed single-phase samples for the manufacture of gas-tight ceramics.

To obtain ceramic samples based on these precursors, two methods were used: thermal treatment in air and thermobaric treatment (TBT). During the formation of ceramic samples, the stage of obtaining nanodispersed single-phase powders of the required composition makes it possible to separate two processes that run in parallel during the solid-phase synthesis – phase formation and sintering. The nanodispersion of the powder of an already prepared composition ensures the production of dense ceramic samples, the sintering of which requires much less time than the sintering of the samples produced by the solid-phase synthesis.

A study of the influence of methods for obtaining ceramics on the morphology of the obtained samples was carried out. A decrease in the average grain size after TBT was found to be almost twofold in comparison with ceramics obtained by sintering in an air atmosphere. The geometric shape of the grains also undergoes significant changes, becoming more faceted.

Two reasons for the increase in the dielectric constant of ceramic samples after TBT were identified. The first one is the distortion of the AO_9 and BO_6 coordination polyhedra, which is most pronounced along the c axis. A significant increase in the Ni(M)–O2b bond length, for example, in the case of the sample containing Cu leads to a noticeable increase in Reε from 600 to 2000. The second reason lies in the increasing the permittivity with decreasing crystallite size, due to the influence of grain boundary effects resulting from the Maxwell-Wagner polarization mechanism.

Supplementary materials

No supplementary materials are available.

Funding

Acknowledgments

Author contributions

Conceptualization: D.Y.A., C.T.I.
Data curation: M.N.V.
Formal Analysis: D.Y.A, M.N.V.
Funding acquisition: D.Y.A.
Investigation: D.Y.A., M.A.A.,
Methodology: D.Y.A., M.A.A., S.A.Y., K.N.I.
Project administration: D.Y.A.
Resources: D.Y.A., C.T.I.
Software: D.Y.A., M.A.A.
Supervision: C.T.I., L.I.A.
Validation: D.Y.A., C.T.I., M.N.V.
Visualization: D.Y.A.
Writing – original draft: D.Y.A.
Writing – review & editing: C.T.I., M.N.V., L.I.A.

Conflict of interest

The authors declare no conflict of interest.

Additional information

Author IDs:

Yulia A. Deeva, Scopus ID 57208866603;
Abdullo A. Mirzorakhimov, Scopus ID 57133042800;
Alexey Yu. Suntsov, Scopus ID 26536695400;
Nadezhda I. Kadyrova, Scopus ID 6701574610;
Nina V. Melnikova, Scopus ID 7003907528;
Tatyana I. Chupakhina, Scopus ID 6602115793.

Websites:

Ural Federal University, https://urfu.ru/en;
Institute of Solid State Chemistry UB RAS, https://www.ihim.uran.ru.

References

1. Ramirez AP, Subramanian MA, et al. Giant dielectric constant response in a copper-titanate. Solid State Commun. 2000;115(5):217–220. doi:10.1016/S0038-1098(00)00182-4
2. Jumpatam J, Putasaeng B, et. al. Improved giant dielectric properties of CaCu$_3$Ti$_4$O$_{12}$ via simultaneously tuning the electrical properties of grains and grain boundaries by F- substitution. RSC Adv. 2017;7(7):4092–4101. doi:10.1039/c6ra27381e
3. Krohns S, Lunkenheimer P, Loidl A. Colossal dielectric constants in La$_{15/8}$Sr$_{1/8}$NiO$_4$. In: Conference on Fundamentals and Technology of Multifunctional Oxide Thin Films; 2009; Strasbourg; FRANCE. doi:10.1088/1757-899x/8/1/012014
4. Lunkenheimer P, Krohns S, et al. Colossal dielectric constants in transition-metal oxides. Eur Phys J Spec Top. 2010;180:61–89. doi:10.1140/epjst/e2010-01212-5
5. Erste A, Kuznik B, et al. Dielectric Properties of CaCu$_3$Ti$_4$O$_{12}$ Ceramic Thin Films. Ferroelectr. 2011;419:14–19. doi:10.1080/00150193.2011.594405
6. Chupakhina TI, Mel'nikova NV, et al. La$_{1.8}$Sr$_{0.2}$Ni$_{0.8}$M$_{0.2}$O$_4$ (M = Fe, Co, or Cu) complex oxides: synthesis, structural characterization, and dielectric properties. Russ J Inorg Chem. 2018;63(2):141–148. doi:10.1134/s0036023618020043
7. Chupakhina TI, Melnikova NV, et al. Synthesis, structure, magnetic behavior and dielectric relaxation of the La$_x$Sr$_{2-x}$Fe$_x$Ti$_{1-x}$O$_4$ (x = 0.5, 0.7) oxide ceramic. J Solid State Chem. 2020;292:121687(1–12). doi:10.1016/j.jssc.2020.121687
8. Rahman Ab, Abu MJ, et al. Effect of Calcination Temperature on Dielectric Properties of CaCu$_3$Ti$_4$O$_{12}$ Ceramics. In: 5th International Conference on Recent Advances in Materials, Minerals and Environment; Ramm. 2016;19:910–915. doi:10.1016/j.proche.2016.03.134
9. Krohns S, Lunkenheimer P, et al. Colossal dielectric constant up to gigahertz at room temperature. Appl Phys Lett. 2009;94(12):3. doi:10.1063/1.3105993
10. Deeva YA, Chupakhina TI, et al. Dielectric properties of new oxide phases Ln$_{0.65}$Sr$_{1.35}$Co$_{0.5}$Ti$_{0.5}$O$_4$ (Ln = La, Nd, Pr) with the K$_2$NiF$_4$ - type structure. Ceram Int. 2020;46(10):15305–15313. doi:10.1016/j.ceramint.2020.03.071
11. Liu XQ, Wu YJ, et al. Temperature-stable giant dielectric response in orthorhombic samarium strontium nickelate ceramics. J Appl Phys. 2009;105(5):4. doi:10.1063/1.3082034
12. Jia BW, Liu XQ, Chen XM. Structure, magnetic and dielectric properties in Mn-substituted Sm$_{1.5}$Sr$_{0.5}$NiO$_4$ ceramics. J Appl Phys. 2011;110(6):7. doi:10.1063/1.3639282
13. Takeda Y, Kanno R. Crystal chemistry and physical properties of La$_{2-x}$Sr$_x$NiO$_4$ (0 ≤ x ≤ 1.6). Mater Res Bull. 1990;25(3):293–306. doi:10.1016/0025-5408(90)90100-G
14. Vashooka V, Girdauskaite E, et al. Oxygen non-stoichiometry and electrical conductivity of Pr$_{2-x}$Sr$_x$NiO$_{4\pm\delta}$ with x = 0–0.5. Solid State Ionics.2006;177(13):1163–1171. doi:10.1016/j.ssi.2006.05.018
15. Oliveira RMPB, Pimentel PM, et al. Microstructural study of neodmium nickelate doped with strontium synthesized by gelatin method. Adv Mater Sci Eng 2013;2013:926540. doi:10.1155/2013/926540
16. Jia BW, Yang WZ et al. Giant dielectric response in (Sm$_{1-x}$Nd$_x$)$_{(1.5)}$Sr$_{0.5}$NiO$_4$ ceramics: The intrinsic and extrinsic effects. J Appl Phys. 2012;112(2):7. doi:10.1063/1.4737775
17. Shi CY, Hu ZB, Hao YM. Structural, magnetic and dielectric properties of La$_{2-x}$Ca$_x$NiO$_{4+\delta}$ (x=0, 0 1, 0 2, 0 3). J Alloys Compd. 2011;509(4):1333–1337. doi:10.1016/j.jallcom.2010.10.030
18. Nirala G, Yadav D, Upadhyay S. Ruddlesden-Popper phase A$_2$BO$_4$ oxides: Recent studies on structure, electrical, dielectric, and optical properties. J Adv Ceram. 2020;9(2):129–148. doi:10.1007/s40145-020-0365-x
19. Chupakhina TI, Melnikova NV, et al. Synthesis, structure and dielectric properties of new ceramics with K$_2$NiF$_4$-type structure. J Eur Ceram Soc. 2019;39(13):3722–3729. doi:10.1016/j.jeurceramsoc.2019.05.018
20. Lou X, Weng WJ, et al. The effects of incomplete combustion on Ba$_2$Ti$_9$O$_{20}$ phase formation in a citrate solution combustion method. Ceram Int. 2009;35(5):1725–1729. doi:10.1016/j.ceramint.2008.09.013
21. Lee MK, Kang S. A study of salt-assisted solution combustion synthesis of magnesium aluminate and sintering behaviour. Ceram Int. 2019;45(6):6665–6672. doi:10.1016/j.ceramint.2018.12.155
22. Montoya JF, Chavarriaga EA, et al. ZnFe$_{2-x}$Cr$_x$O$_4$ ferrites (x=0.0-2.0) by solution-combustion synthesis using glycine as a fuel: influence of Cr^{3+} doping. Int J Self Propag High Temp Synth. 2020;29(4):243–245. doi:10.3103/s1061386220040081
23. Chupakhina TI, Gyrdasova OI, et al. New ways to synthesize multifunctional ceramics La$_{2-x}$Sr$_x$NiO$_4$. Russ J Inorg Chem. 2015;60(10):1184–1192. doi:10.1134/s0036023615100058

24. Boehm E, Bassat J-M et al. Oxygen transport properties of $La_2Ni_{1-x}Cu_xO_{4+\delta}$ mixed conducting oxides. Solid State Sci. 2003;5(7):973–981. doi:10.1016/S1293-2558(03)00091-8

25. Tarutin AP, Lyagaeva JG, et al. Cu-substituted $La_2NiO_{4+\delta}$ as oxygen electrodes for protonic ceramic electrochemical cells. Ceram Int. 2019;45(13):16105–16112. doi:10.1016/j.ceramint.2019.05.127

26. Filonova EA, Pikalova EYu, et al. Crystal structure and functional properties of $Nd_{1.6}Ca_{0.4}Ni_{1-y}Cu_yO_{4+\delta}$ as prospective cathode materials for intermediate temperature solid oxide fuel cells. Int J Hydrog Energy. 2021;46(32):17037–17050. doi:10.1016/j.ijhydene.2020.10.243

27. Kadyrova NI, Mel'nikova NV, et al. Effect of high pressures and temperatures on the structure and properties of $CaCu_3Ti_4O_{12}$. 2016;52:1051–1054. doi:10.1134/S0020168516100083

28. Chupakhina TI, Deeva YA, et al. Synthesis, structure and dielectric properties of new oxide compounds $Ln_{1-x}Sr_{1+x}Cu_{x/2}Ti_{1-x/2}O_4$ (Ln = La, Pr, Nd) belonging to the structural type of K_2NiF_4. Mendeleev Commun. 2019;29(3):349–351. doi:10.1016/j.mencom.2019.05.037

29. Fan XC, Chen XM, Liu XQ. Structural dependence of microwave dlielectric properties of $SrRAIO_4$ (R = Sm, Nd, La) ceramics: Crystal structure refinement and infrared reflectivity study. Chem Mater. 2008;20(12):4092–4098. doi:10.1021/cm703273z

30. Shannon RD. Revised effective ionic radii and systematic studies of interatomic distances in halides and chalcogenides. Acta Crystallograph Sec A. 1976;32(5):751–767. doi:10.1107/S0567739476001551

31. Goncharov VS, Ryzhkovskii VM. Thermobaric treatment induced changes in the structure and magnetic properties of manganese antimonide. Techn Phys Lett. 2001;27(7):546–547. doi:10.1134/1.1388938

32. Vasala S, Karppinen M. $A_2B'B''O_6$ perovskites: A review. Prog Solid State Chem. 2015;43(1–2):1–36. doi:10.1016/j.progsolidstchem.2014.08.001

33. Lombardo SJ, Shende RV, Krueger DS. The effect of processing conditions on the porosity and electrical properties of IBLC materials. Ceram Mater Multilayer Electron Devices. 2003;150:43–51. doi:10.1016/j.ceramint.2013.08.123

34. Salame P, Drai R et al. IBLC effect leading to colossal dielectric constant in layered structured Eu_2CuO_4 ceramic. Ceram Int. 2014;40(3):4491–4498. doi:10.1016/j.ceramint.2013.08.123